











## Changes in land use and management led to a decline in Eastern Europe's terrestrial carbon sink

Karina Winkler <sup>1,2</sup>✉, Hui Yang<sup>3</sup>, Raphael Ganzenmüller <sup>4</sup>, Richard Fuchs <sup>1</sup>, Guido Ceccherini <sup>5</sup>, Grégory Duveiller <sup>3</sup>, Giacomo Grassi <sup>5</sup>, Julia Pongratz<sup>4,6</sup>, Ana Bastos <sup>3</sup>, Anatoly Shvidenko <sup>7</sup>, Arnan Araza<sup>2</sup>, Martin Herold<sup>2,8</sup>, Jean-Pierre Wigneron <sup>9</sup> & Philippe Ciais <sup>10</sup>

Land-based mitigation is essential in reducing net carbon emissions. Yet, the attribution of carbon fluxes remains highly uncertain, in particular for the forest-rich region of Eastern Europe (incl. Western Russia). Here we integrate various data sources to show that Eastern Europe accounted for an above-ground biomass carbon sink of -0.41 gigatons of carbon per year over the period 2010–2019, that is 78% of the entire European carbon sink. We find that this carbon sink is declining, mainly driven by changes in land use and land management, but also by increasing natural disturbances. Based on a random forest model, we show that land use and management changes are main drivers of the declining carbon sink in Eastern Europe, although soil moisture variability is also important. Specifically, the saturation effect of tree regrowth in abandoned agricultural areas, combined with increasing wood harvest removals, particularly in European Russia, contributed to the decrease in the Eastern European carbon sink.

<sup>1</sup>Land Use Change & Climate Research Group, IMK-IFU, Karlsruhe Institute of Technology (KIT), Garmisch-Partenkirchen, Germany. <sup>2</sup>Laboratory of Geoinformation and Remote Sensing, Wageningen University & Research (WUR), Wageningen, The Netherlands. <sup>3</sup>Max Planck Institute for Biogeochemistry (MPI-BGC), Jena, Germany. <sup>4</sup>Department of Geography, Ludwig-Maximilians-Universität München, Munich, Germany. <sup>5</sup>Joint Research Centre of the European Commission, Ispra, Italy. <sup>6</sup>Max Planck Institute for Meteorology, Hamburg, Germany. <sup>7</sup>International Institute for Applied Systems Analysis IIASA, Laxenburg, Austria. <sup>8</sup>Helmholtz Centre Potsdam, GFZ German Research Centre for Geosciences, Potsdam, Germany. <sup>9</sup>ISPA, INRAE Bordeaux, Université de Bordeaux, Villenave d'Ornon, France. <sup>10</sup>Laboratoire des Sciences du Climat et de l'Environnement, LSCE, Université Paris-Saclay, Saint-Aubin, France. ✉email: [karina.winkler@kit.edu](mailto:karina.winkler@kit.edu)

Carbon sequestration from the terrestrial biosphere contributes to climate change mitigation. Globally, the terrestrial biosphere absorbs almost one-third of the total anthropogenic CO<sub>2</sub> emissions<sup>1,2</sup>. After the Paris Agreement, many countries proclaimed ambitious plans to achieve neutral net greenhouse gas emissions<sup>3</sup>—a target that can only be reached by reducing emissions in combination with increasing “negative” emissions from land-based carbon uptake<sup>4</sup>. However, despite the societal relevance of land-based mitigation, there are still large uncertainties when measuring both the amount of carbon that is currently released and sequestered by the land surface as well as estimating the additional carbon that the land could potentially further take up<sup>1,5</sup>. These uncertainties stem from the use of diverse methodologies, differences in underlying land use/cover datasets, and divergent representations of processes within models<sup>1</sup>.

Methods for estimating land carbon fluxes are divided into top-down and bottom-up (see Fig. 1). Top-down atmospheric inversions rely on the analysis of atmospheric CO<sub>2</sub> concentrations gradients to infer the accumulated effect of all CO<sub>2</sub> sources and sinks after removing the signal of fossil CO<sub>2</sub> emissions<sup>5</sup>. Bottom-up approaches cover ground-based inventories, satellite-based estimates of biomass carbon changes, and models. Inventories are performed in regular multi-year periods by national agencies and form the base of UNFCCC reporting<sup>6</sup>. However, they differ by the density of samples, by the component measured (e.g., soil carbon or biomass change), and by accounting choices such as how natural disturbances are considered<sup>3</sup>. Satellite-based measurements recently made it possible to infer biomass changes, but only few global products are available<sup>7–9</sup>. On the other hand, there are many models ranging from simple data-driven models<sup>10</sup> to process-based models such as Dynamic Global Vegetation Models (DGVMs)<sup>1,11</sup>. Some models are specialized in certain components of the terrestrial carbon balance such as semi-empirical bookkeeping models<sup>1</sup> which are used to assess emissions and removals from land-use change and land management in global assessments of the carbon budget.

At the global scale, atmospheric inversions quantify the net CO<sub>2</sub> flux exchanged between terrestrial ecosystems and the atmosphere but do not separate them into components or drivers. They give a global sink of ~1.3 Gt C a<sup>-13</sup> over managed lands for 2007–2017, while all national inventories provided a sink of ~0.5 Gt C a<sup>-1</sup> for 2000–2020<sup>12</sup>. Recent satellite-based biomass estimates account for a net carbon sink of 0.2 to 0.9 Gt C a<sup>-1</sup> for 2000–2019<sup>13</sup>.

The basis for accurate estimates of carbon fluxes is knowledge and attribution of the underlying man-made and environmental drivers. One major anthropogenic driver of land carbon change (from land use and management) is agricultural land use change, with agricultural expansion leading to a carbon source (loss of biomass)<sup>1,14</sup> and agricultural abandonment leading to a carbon sink (enhanced woody biomass and soil carbon due to regrowth)<sup>1,15,16</sup>. Forestry is another essential land management driver with wood harvest (removal of biomass) leading to enhanced carbon emissions and thus weaker forest sinks<sup>14</sup>. Further, fires as mostly natural disturbance to forests in Europe, reduce the carbon sink<sup>17</sup>. Environmental factors such as atmospheric CO<sub>2</sub> and nitrogen deposition have been found to enhance the land-based carbon sink<sup>18,19</sup>, whereas the influence of temperature, precipitation, or soil moisture on the land-based carbon sink can be positive or negative, and involve complex land-atmosphere feedbacks<sup>20</sup>.

Although the Northern Hemisphere is a large terrestrial carbon sink according to observational and modeling approaches<sup>21</sup>, at continental and sub-continental scale, there is no consensus about the magnitude of the carbon uptake or release between inventories and research-based methods including atmospheric inversions, ecosystem models, and satellite-based biomass carbon storage<sup>5,22</sup>. Even in Europe, where the density of observational data is comparatively high from a global perspective, deviation between estimates are large and remain poorly understood<sup>23</sup>. Studies focussing on the European carbon balance indicated a large spread in the continental carbon sink with values of ~0.20 Gt C a<sup>-1</sup> for 2006–2015 (based on inversions)<sup>24</sup>,

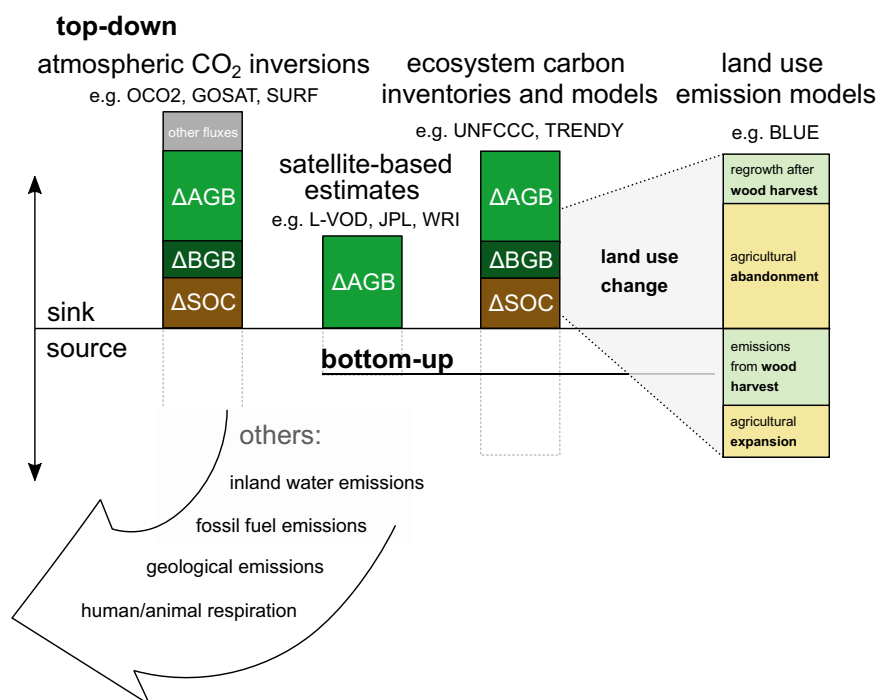


**Fig. 1 Carbon flux components from different datasets and models.** Overview of carbon flux components (ΔAGB: Above-ground biomass, ΔBGB: Below-ground biomass, ΔSOC: Soil organic carbon) as addressed by different datasets and models with examples used in this study.

$\sim 0.30 \text{ Gt C a}^{-1}$  for 2010–2015 (based on in-situ  $\text{CO}_2$  and passive microwave measurements)<sup>25</sup> or  $\sim 0.95 \text{ Gt C a}^{-1}$  for 2003–2010 (based on inversions)<sup>22</sup>.

When examining Europe's land-based carbon sink, Eastern Europe is of particular interest. Many studies suggest that densely forested Eastern Europe (see Supplementary Fig. 1) has enormous potential for climate mitigation<sup>22,23,26</sup>. However, there are large uncertainties in its carbon balance and only very few in-situ observational data<sup>23</sup>. This lack of reliable inventory and flux data has motivated the application of satellite-driven methods for quantifying the carbon uptake in this region. Eastern Europe is not only an extensively forested area that should foster a potentially large carbon uptake, it also has been affected by major land use and management changes through the recent history of political and institutional upheaval, distinctly from Western Europe. The collapse of the Soviet Union generated land tenure changes, a transition to open-market economies, and several economic crises, all of which have triggered dramatic changes in forest disturbances and recovery rates<sup>27</sup> but also in agricultural land management<sup>28</sup>. Furthermore, Eastern European forests are prone to natural disturbance and weather extremes, which lead to frequent fires, storms, and insect outbreaks<sup>29,30</sup>. Yet, forests across Russia appear to have continued to act as a larger carbon sink than previously reported<sup>31</sup>. The carbon sink of Siberian forests, however, was found to be extremely vulnerable to climate-induced disturbances such as fire and drought, which caused losses of above-ground carbon during the last decade<sup>32</sup>. Due to its high relevance for European climate mitigation, the lack of conclusive estimates on the mean and trend of the carbon sink as well as the unique interplay of socio-economic and climatic drivers, the carbon balance of Eastern Europe is the focus of this study. Here, Eastern Europe consists of 13 countries: Belarus, Bulgaria, Czech Republic, Estonia, Hungary, Latvia, Lithuania, Moldova, Poland, Romania, Slovakia, Ukraine, and western Russia (up to the Ural Mountains; in accordance to commonly used geographical classifications of the United Nations Statistical Commission, CIA World Factbook or EuroVoc thesaurus by the Publications Office of the European Union). For context, we also compare our new results over Eastern Europe with published estimates of other regions of Europe.

In this paper, we take stock of new observation-based approaches (satellite-derived biomass change, atmospheric inversions assimilating satellite  $\text{CO}_2$  data over regions where there are no surface stations) and improved models for land use change fluxes driven by updated input data. The objectives of this study are (1) to quantify the land carbon uptake in Eastern Europe in the last decade, (2) to identify spatial and temporal patterns, and (3) to attribute possible underlying drivers to changes in land use, management, and in environmental variables.

## Results and discussion

**The role of the Eastern European carbon sink.** By comparing estimations of the land carbon uptake from different data sources— $\text{CO}_2$  inversions, satellite-based biomass change, land use change models, and inventories (see Table 1)—we found that Eastern Europe holds the largest share (on average  $\sim 65 \pm 15\%$ ) of the total European carbon sink, in all the data streams (see Fig. 2 and Table 2).

According to the satellite-based above-ground biomass (AGB) change estimates from L-VOD, the annual biomass carbon uptake of the Eastern European region is  $\sim 0.45 \pm 0.10 \text{ Gt C a}^{-1}$  during 2010–2019—around three times as much as taken up by Northern, Western and Southern Europe together. Satellite-based AGB estimates from WRI indicate a gross biomass carbon sink of

$\sim 0.38 \text{ Gt C a}^{-1} \pm 0.10 \text{ Gt C a}^{-1}$ . Considering the areas of annual carbon increase from the third satellite-based approach by JPL, we obtain gross carbon sink estimates of  $\sim 0.32 \pm 0.08 \text{ Gt C a}^{-1}$  (see Table 2). These satellite-derived estimates of the AGB carbon sink are in line with the net  $\text{CO}_2$  sink estimated from top-down inversions (SURF, GOSAT, OCO2), ranging from  $\sim 0.32 \pm 0.04$  to  $\sim 0.52 \pm 0.10 \text{ Gt C a}^{-1}$ . Because inversions' net fluxes also include  $\text{CO}_2$  fluxes from non-forest ecosystems and soil carbon changes in forests, this suggests that most of the net  $\text{CO}_2$  sink from inversion lies in an increasing forest AGB.

Based on UNFCCC national inventories, we note a smaller mean carbon sink in the land use, land use change and forestry (LULUCF) sector ( $\sim 0.20 \pm 0.13 \text{ Gt C a}^{-1}$ ) compared to inversion-net land  $\text{CO}_2$  flux and L-VOD-based biomass carbon increase. In addition, the LULUCF sink of Eastern Europe is ten times larger than the overall net sink caused by land use change alone as simulated by the land use emission model BLUE ( $\sim 0.02 \pm 0.01 \text{ Gt C a}^{-1}$ ). The gross carbon increase caused by land use change (agricultural abandonment) in BLUE, however, adds up to  $\sim 0.11 \pm 0.01 \text{ Gt C a}^{-1}$ , around half of the reported carbon sink from LULUCF in Eastern Europe (see Fig. 2). Greenhouse gas emissions from wood harvesting and agricultural land use change, which act as sources, partially offset this gross carbon sink from agricultural abandonment.

Overall, the persistent deviations between the carbon sink estimates from different data streams can be explained by four reasons. First, the datasets differ in terms of methodology and incorporate different definitions (e.g., regarding land cover), comprise different carbon components (soil organic carbon, above-ground or total vegetation biomass) and include very different approaches (top-down vs. bottom-up)<sup>5,33</sup>. Second, distinct time periods lead to discrepancies due to high inter-annual variability of net carbon fluxes. Third, the models are tailored to different drivers of carbon change such as altering climate and environmental factors, land use, or land management. Fourth, whether the focus is on calculating gross or net carbon fluxes, may cause major divergence, as shown for the land use emission estimates from the BLUE model (compare BLUE-gross and BLUE-net in Fig. 2).

Overall, the Eastern European AGB carbon sink, as derived from both top-down and bottom-up approaches (here: SURF, GOSAT, OCO2, L-VOD, JPL, WRI) is on average  $\sim 0.41 \text{ Gt C a}^{-1} \pm 0.09 \text{ Gt C a}^{-1}$ , that is 78% of the entire carbon sink of the European continent. Considering only bottom-up, observation-based AGB change datasets with matching reference period (2010–2019), JPL and WRI gross and L-VOD-based estimates, we find that the AGB carbon sink of Eastern Europe is  $\sim 0.38 \text{ Gt C a}^{-1}$  ( $\pm 0.07 \text{ Gt C a}^{-1}$ ). From this, LULUCF contributes with  $\sim 53\%$  according to UNFCCC and land use change with  $\sim 29\%$  according to the BLUE model (when gross carbon sink estimates are considered).

**Decline of the Eastern European carbon sink.** We find that the land carbon sink in Eastern Europe declined over the period 2010–2019. Mean annual carbon uptake from L-VOD is almost 20% lower in 2015–2019 ( $\sim 0.37 \pm 0.04 \text{ Gt C a}^{-1}$ ), compared to 2010–2019 ( $\sim 0.45 \pm 0.10 \text{ Gt C a}^{-1}$ ). This decline is also indicated from satellite inversions. The OCO-2 inversion, which covers the period 2015–2019, shows a lower carbon sink ( $\sim 0.32 \pm 0.04 \text{ Gt C a}^{-1}$ ) than the SURF and GOSAT inversions ( $\sim 0.51 \pm 0.10 \text{ Gt C a}^{-1}$ ), which cover the periods 2010–2018 and 2010–2015, respectively. This difference, however, may also be an effect of the different atmospheric observations used.

According to UNFCCC annual reports of Eastern Europe (see Fig. 3), Russia, Belarus, and Poland are the biggest contributors to

**Table 1 Overview of carbon flux datasets.**

Dataset abbreviation	Description	Method type	Spatial resolution	Temporal coverage	Source
<b>SURF</b>	Assimilation of CO <sub>2</sub> surface measurements in atmospheric transport model from Copernicus Atmosphere Monitoring Service (CAMS)	Top-down (Atmospheric inversion)	1.875° × 3.75°	2010–2018	CAMS <sup>59</sup>
<b>GOSAT</b>	CO <sub>2</sub> column retrievals from GOSAT satellite in atmospheric transport model from CAMS	Top-down (Atmospheric inversion)	1.875° × 3.75°	2010–2015	CAMS <sup>59</sup>
<b>OCO2</b>	CO <sub>2</sub> column retrievals from OCO-2 satellite in atmospheric transport model from CAMS	Top-down (Atmospheric inversion)	1.875° × 3.75°	2015–2018	CAMS <sup>59</sup>
<b>L-VOD</b>	Regression of spatial above-ground biomass (AGB) and L-band vegetation optical depth (L-VOD) derived from the Soil Moisture and Ocean Salinity (SMOS) satellite	Bottom-up (Satellite-based estimates of AGB change)	0.25°	2010–2019	INRAE BORDEAUX <sup>38</sup>
<b>JPL Jet Propulsion Laboratory</b>	Machine learning model trained with ground-based forest inventories and airborne LIDAR and multiple RS data applied to infer biomass	Bottom-up (Satellite-based estimates of AGB change)	0.1°	2010–2019	Xu et al. <sup>13</sup>
<b>WRI World Resources Institute</b>	Carbon flux model (integration of ground and Earth observation data)	Bottom-up (Satellite-based estimates of AGB change)	0.1°	2010–2019	Adapted from Harris et al. <sup>7</sup>
<b>UNFCCC</b>	National greenhouse gas (GHG) inventories, net CO <sub>2</sub> emissions/removals from land use, land use change, and forestry (LULUCF).	Bottom-up (National inventories)	country-scale	2010–2019	UNFCCC <sup>71,72</sup>
<b>EFISCEN</b>	Carbon stocks of trees from European Forest Information SCENario Model (EFISCEN) based on national inventories	Bottom-up (Forest carbon model)	country-/plot-scale <sup>a</sup>	2010–2018	EFI <sup>86,87</sup> as applied in VERIFY <sup>5</sup>
<b>CBM</b>	Simulated forest carbon dynamics from the Carbon Budget Model (CBM)	Bottom-up (Forest carbon model)	country-scale <sup>a</sup>	2010–2015	Kurz et al. <sup>88</sup> as applied in VERIFY <sup>5,89</sup>
<b>BLUE</b>	Bookkeeping model (BLUE): Net CO <sub>2</sub> flux only from land use/cover change	Bottom-up (Land use carbon model)	0.25° (from original 0.01°)	2010–2019	Ganzenmüller et al. <sup>74</sup>

<sup>a</sup>Datasets (incl. abbreviations and characteristics) used for comparing estimates of land-based carbon uptake over Europe.

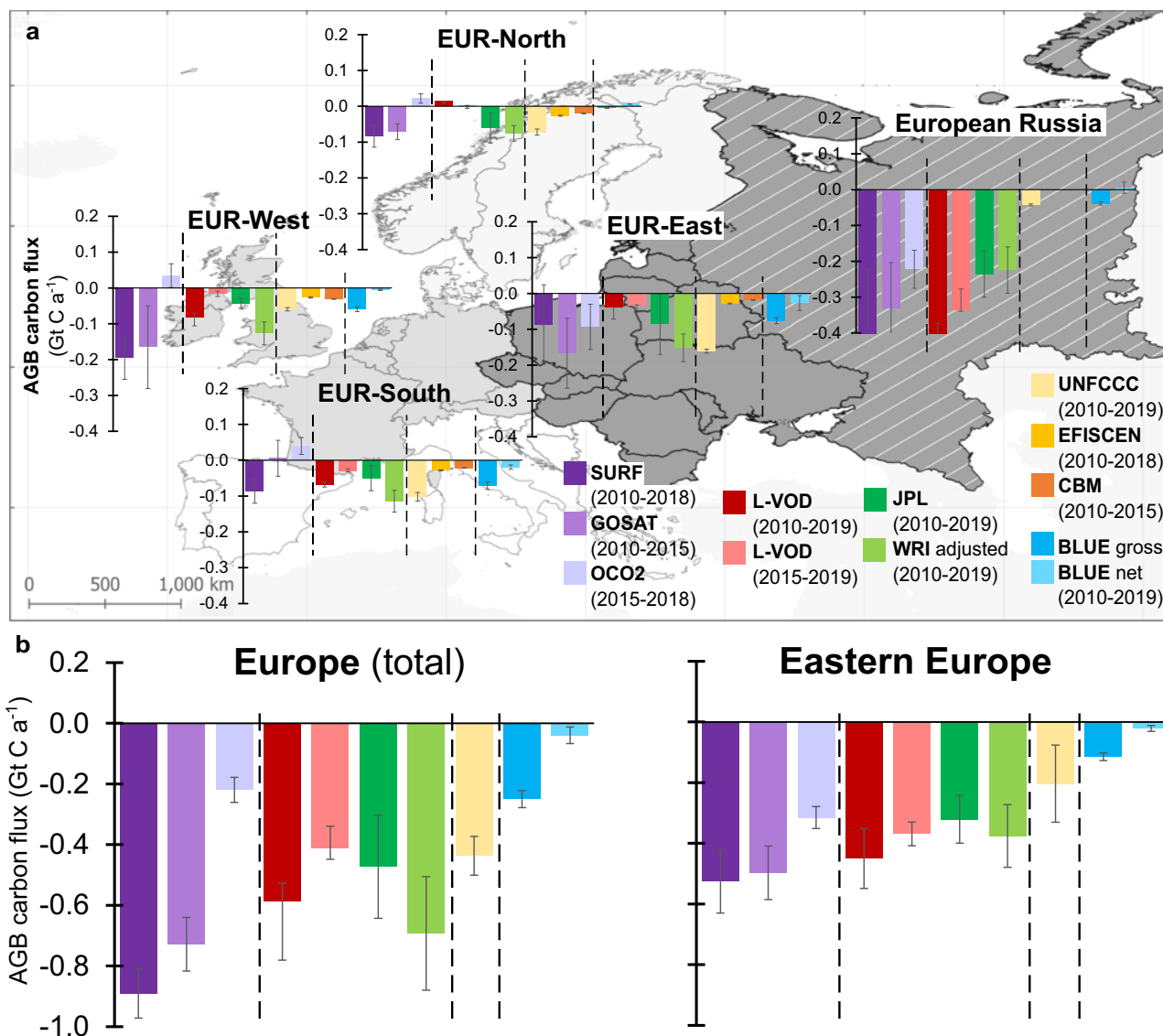


**Fig. 2 Carbon flux estimates for European regions.** Average land carbon flux (in  $\text{Gt C a}^{-1}$ ) from inversions (SURF, GOSAT, OCO2), AGB sink estimates (L-VOD, JPL\*\*, WRI\*\*), forest ecosystem models and inventories (EFISCEN, CBM, UNFCCC) and land use bookkeeping model BLUE between 2010 and 2019 **a** for different regions in Europe (see Supplementary Table 1) and **b** for Eastern Europe compared to entire Europe (aggregated). Negative values represent a land carbon sink, positive values a land carbon source. Eastern Europe comprises EUR-East and European Russia. Error bars display the standard deviations of the estimates as a measure of the variability across time (see Supplementary Table 2). \*\* refers to gross carbon sink estimates.

**Table 2 Carbon flux estimates for European regions.**

Data	SURF	GOSAT	OCO2	L-VOD	JPL <sup>a</sup>	WRI <sup>a</sup>	UNFCCC	BLUE <sup>o,a</sup>
Period	2010-18	2010-15	2015-18	2010-19	2010-2019	2010-19	2010-19	2010-19
North	-0.08	-0.07	0.02	0.02	-0.06	-0.08	-0.07	-0.01
West	-0.20	-0.17	0.04	-0.08	-0.04	-0.13	-0.06	-0.06
South	-0.09	0.01	0.04	-0.07	-0.05	-0.11	-0.10	-0.07
East	-0.09	-0.17	-0.09	-0.04	-0.09	-0.15	-0.16	-0.08
Russia	-0.44	-0.33	-0.22	-0.41	-0.24	-0.22	-0.04	-0.04
<b>EE</b>	<b>-0.53</b>	<b>-0.50</b>	<b>-0.32</b>	<b>-0.45</b>	<b>-0.32</b>	<b>-0.38</b>	<b>-0.20</b>	<b>-0.11</b>
EE share	59%	68%	143%	77%	68%	54%	47%	46%
Europe	-0.89	-0.73	-0.22	-0.59	-0.47	-0.69	-0.44	-0.25

Average land carbon flux (in  $\text{Gt C a}^{-1}$ ) from different datasets (see Table 1 and Fig. 2) for European regions (see Supplementary Table 1). Negative values indicate an atmospheric  $\text{CO}_2$  sink or an increase in land C stock. Uncertainties in form of standard deviations are given in Supplementary Table 2. Net AGB carbon fluxes (if available) are given in Supplementary Table 3. Values for the study region Eastern Europe (EE: East + Russia) are displayed in bold. EE share shows the share of the Eastern European (EE) in the total European (Europe) carbon fluxes.

<sup>a</sup>Includes not only AGB, but also below-ground biomass (BGB) and soil organic carbon (SOC).

<sup>o</sup>Refers to gross carbon sink estimates.

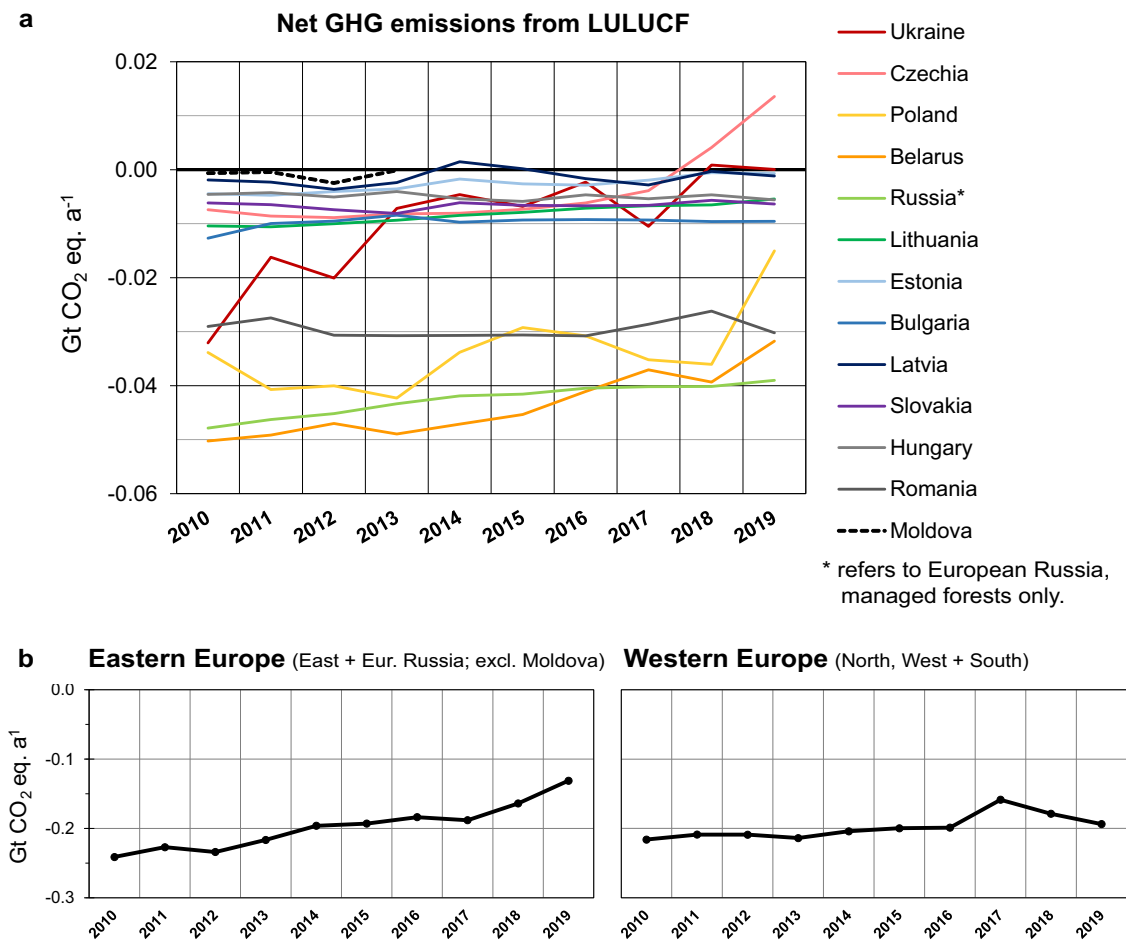


**Fig. 3 Carbon fluxes from land use, land use change and forestry in Eastern Europe.** Annual carbon balance from land use, land use change, and forestry **a** by country in Eastern Europe during 2010–2019 **b** for regions of Eastern and Western Europe from aggregated country data (UNFCCC). Negative values represent a land carbon sink, positive values represent a land carbon source. Note that no uncertainty information is available for these data. \*Values for European Russia contain carbon fluxes from forestry only (National Inventory Reports).

the land carbon sink. Overall, the annual net land carbon sink from the LULUCF sector has decreased during the last decade (–52% decrease relative to 2010). The highest rates of decrease can be found in Czechia, which even turned from a net carbon sink to a net carbon source (decrease of >100%), Ukraine (decrease of 100%), and Poland (decrease of 65%). A declining trend can also be found in the net carbon sink from land use change, as derived from the BLUE model (see Supplementary Fig. 2). The Eastern European net carbon sink from land use change alone decreased by ~92% ( $\sim 0.03 \text{ Gt C a}^{-1} \pm 0.01 \text{ Gt C a}^{-1}$ ) during 2010–2019. This is due to increasing emissions from wood harvest (+47%) and agricultural expansion (+12%) as well as decreasing carbon sequestration from agricultural land abandonment (–11%). This suggests that changes in land use and management have substantially contributed to the decreasing AGB carbon sink in Eastern Europe during the last decade.

Our observations are consistent with other studies. Deng et al.<sup>3</sup> compared global inversion models with UNFCCC inventories and found a decreasing land carbon sink, however only covering the EU-27 and U.K. Early signs of a carbon sink saturations in European forests have been observed from a previous study<sup>34</sup>, which found that the declining trend of the Eastern European carbon sink became evident after the early 2000s. Further, a significant negative anomaly of net primary productivity of forests in European Russia was observed due to the effects of a strong heatwave in 2010<sup>35</sup>. The drought of 2010 also caused an

enormous rise of forest fires in European Russia, a substantial source of carbon emissions<sup>36</sup>. In addition, an increasing rate of wood harvest and disturbances by forest fires have been found to cause a decrease of the forest carbon sink in Russia since 2008<sup>37</sup> and in the Siberian forests<sup>32</sup>. More frequent temperature extremes and days without precipitation have been linked to lower growing stock in forests of southern European Russia<sup>31</sup>. In summary, there are first indications that the declining trend of the Eastern European carbon sink during 2010–2019 was caused by a combined effect of increasing wood harvest and climate-driven natural disturbances.

**Spatial patterns of the Eastern European carbon sink.** The spatial pattern of the Eastern European carbon sink was derived by comparing only changes of the satellite-derived biomass estimates JPL<sup>13</sup>, L-VOD<sup>38</sup>, and WRI<sup>7</sup> because of their similarity in methodology (bottom-up, satellite-based), spatial resolution, temporal coverage and the target component from the carbon cycle, above-ground biomass (AGB). We find high agreement on a carbon sink along the Ural Mountains, in the border between Belarus, Ukraine and Russia as well as on the Kola peninsula in north-western Russia (see Fig. 4).

Considering both the level of agreement and the strength of the carbon sink from the three estimates where they agree on the sign of AGB change (see Fig. 4b, c), we find that the southern Ural



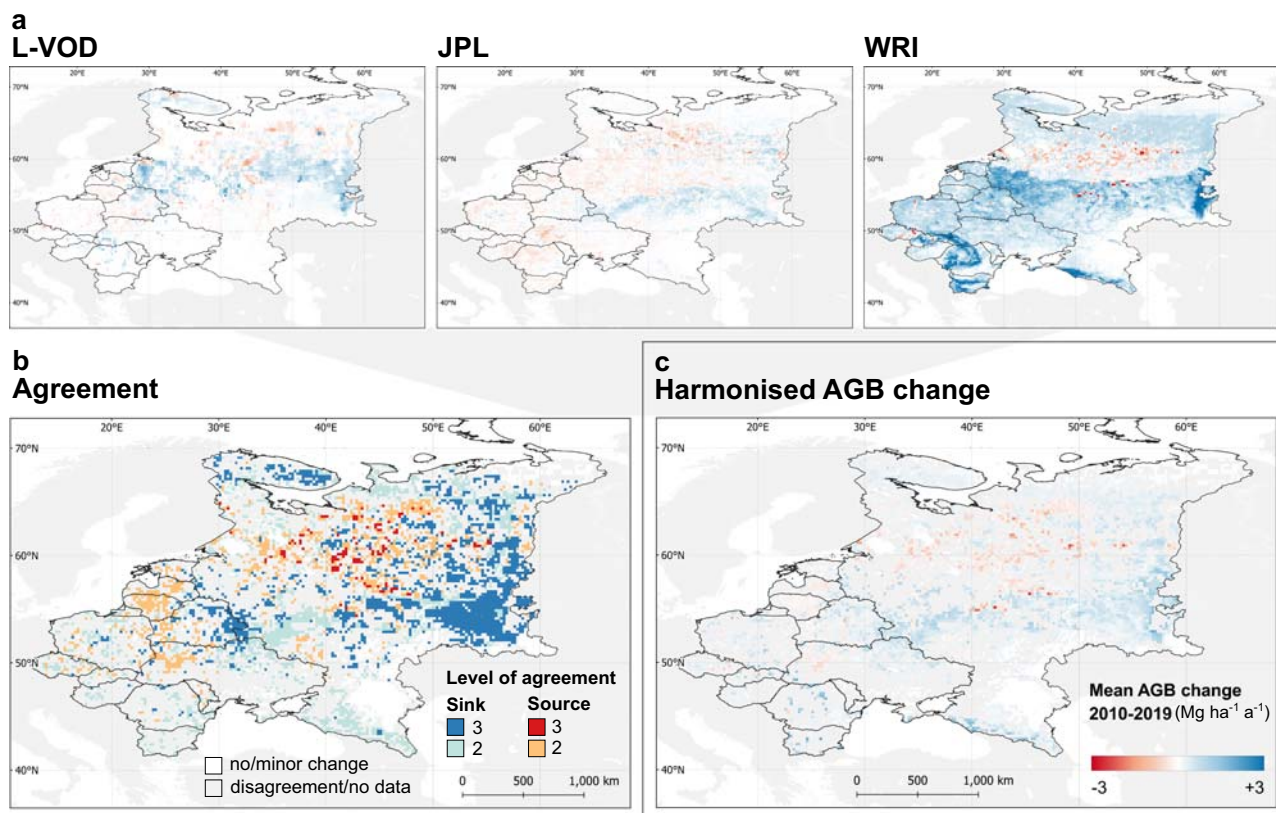


**Fig. 4** Spatial patterns of AGB change in Eastern Europe during 2010–2019. **a** AGB change in Eastern Europe during 2010–2019 from individual datasets: L-VOD, JPL, and WRI. **b** Data agreement on carbon gains (source) and losses (sink). Sources are defined by  $\Delta\text{AGB} < -0.05 \text{ Mg C ha}^{-1} \text{ a}^{-1}$ , sinks by  $\Delta\text{AGB} > 0.05 \text{ Mg C ha}^{-1} \text{ a}^{-1}$ . Levels of agreement represent the number of agreeing datasets. **c** Harmonized mean AGB change from agreeing datasets. The harmonized mean AGB change was derived for all dataset that agree on either a carbon source or sink in areas with an agreement level of at least 2. Areas of disagreement are displayed in gray.

Mountains, and the border region of Russia, Belarus, and Ukraine were hot spots of the Eastern European carbon uptake during 2010–2019. At the same time, scattered hot spots of carbon sources are located in central to northern European Russia, north of 55°N.

Reuter et al. (2017) suggested the largest carbon sink area to be further north in European Russia, where we locate scattered carbon sources. However, their findings referred to a previous period and are therefore not directly comparable<sup>23</sup> and were based on X-band VOD which is prone to saturation effects and shows implausible carbon change in some regions. A recent satellite-based study on the carbon budget of the top five CO<sub>2</sub> emitters shows that European Russia comprises a large carbon sink, whose location corresponds to the hot spot regions presented in this study<sup>39</sup>. Watts et al.<sup>40</sup> analyzed the carbon uptake in the arctic-boreal region and found a large carbon sink in the Eurasian boreal zone, which notably overlaps with our results at the Ural Mountains in European Russia.

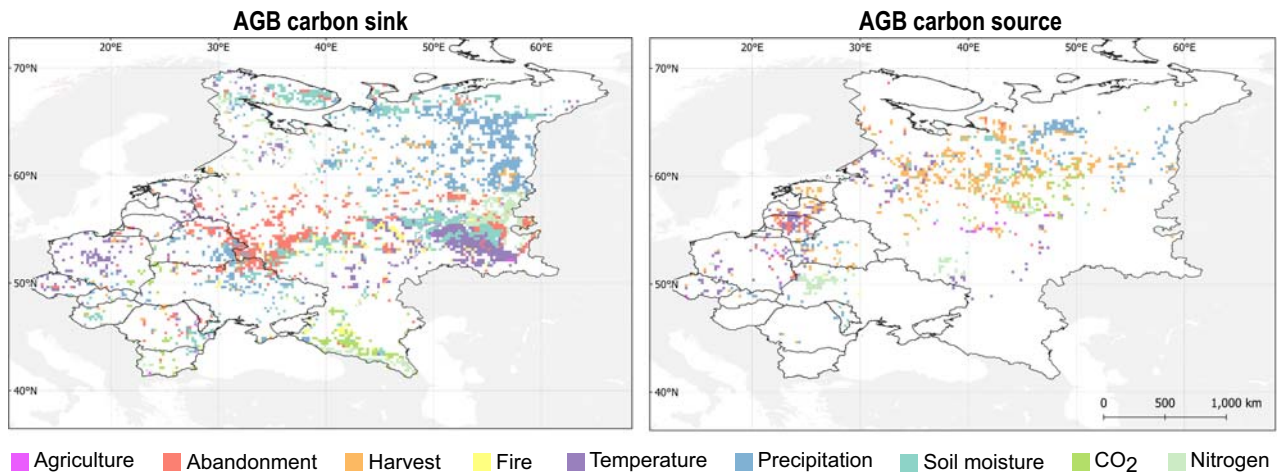
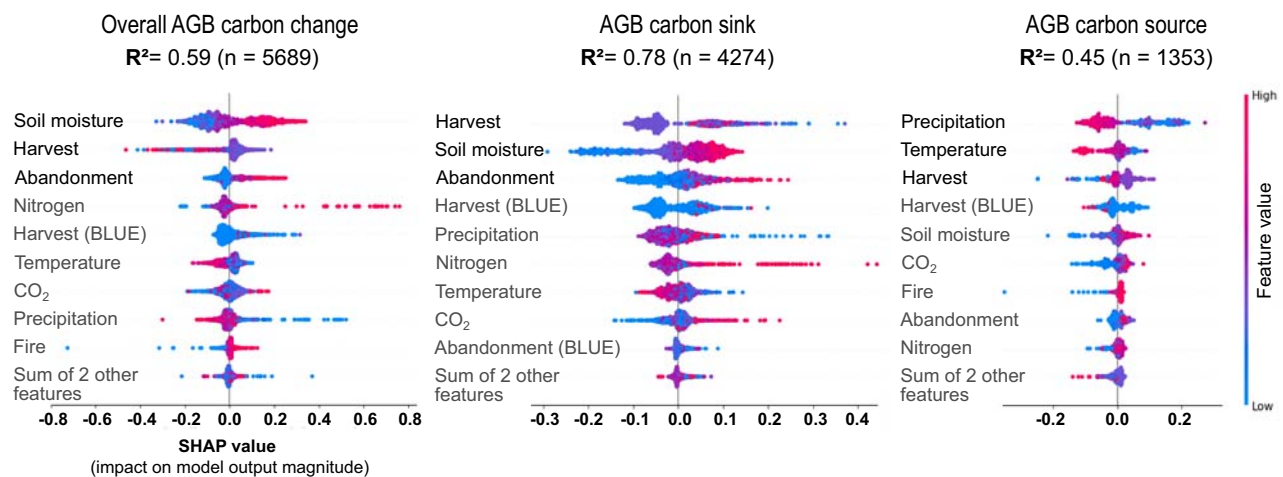
#### Underlying drivers of the Eastern European carbon uptake.

The net CO<sub>2</sub> sink and AGB changes are influenced on the one hand by land use change (the conversion of one land use class to another), by management changes (within one land use class), and by changes in environmental drivers on the other. To find out where exactly which factors have caused land carbon changes in Eastern Europe during recent years, we analyzed the trends of these individual possible drivers and compared them with a harmonized map of AGB change based on JPL, L-VOD, and WRI. For land use and management drivers of AGB changes we

consider the land use-based carbon fluxes from the BLUE model (including agricultural expansion, wood harvest, and agricultural land abandonment), forest harvest change, and the fraction of cropland abandonment. Environmental and climate factors include changes in land surface temperature, precipitation, soil moisture, fires, atmospheric CO<sub>2</sub> concentration, and nitrogen deposition. The trends of all possible driving factors of AGB change in Eastern Europe during 2010–2019 are displayed in Supplementary Fig. 3.

By matching the trends of the driver indicators to AGB change from all three satellite-based AGB estimates (JPL, L-VOD, and WRI) using a random forest model, we find that land use change, in particular cropland abandonment and subsequent regrowth processes, coincide with the hot spot areas of the Eastern European carbon sink (see Fig. 5a). The fraction of formerly abandoned land is high in the carbon sink hot spot region of the border between Russia, Belarus and Ukraine and in central European Russia. As demonstrated by previous studies, cropland abandonment has mainly occurred in the early 1990s after the fall of the Soviet Union<sup>15,41</sup>. Thus, those abandoned lands have already sequestered considerable quantities of carbon before 2010. Nevertheless, carbon storage on formerly abandoned areas still plays an important role for the Eastern European AGB change and, in fact, an increase of AGB is yet to happen as large parts of abandoned lands continue to evolve to closed forests<sup>26</sup>. Therefore, land abandonment is still a major contributor to the Eastern European carbon uptake during 2010–2019 ( $\sim 0.11 \text{ Gt C a}^{-1}$  from BLUE), contributing about 1/3 to 1/5 to the net carbon exchange.

The decreasing trend of the carbon sink shown by the mean of the three satellite AGB change records and land use inventories

**a Trend pattern matching****b Variable importance from random forest model**

**Fig. 5 Drivers of AGB carbon change in Eastern Europe during 2010–2019.** **a** Trend pattern matching: Factors with the highest/lowest standardized trend during 2010–2019 were selected and classified as possible drivers. **b** Random forest regression model: Feature importance based on the Shapley values of all driver indicators for AGB carbon change, AGB sink and source areas.

are partly explicable by the decreasing trend in the abandonment sink as given by the BLUE model (see Supplementary Fig. 2). This may be attributable to a slow-down of the effects of the carbon sequestration following land abandonment. A decrease of the carbon sequestration in soils from around 15 years after agricultural abandonment in Russia has been reported by several studies<sup>42–44</sup>. Further, as re-growing trees on formerly abandoned land turn to denser forests, first signs of a saturation effect of the carbon accumulation—a decreased carbon absorption—are occurring<sup>34,37,45</sup>. Under these circumstances, the carbon sink on abandoned areas is expected to further decrease in the future. Interestingly, abandoned lands, although encroached by woody vegetation, often still have a legal designation for crop production and could be recultivated any time in the near future. A partial revival of agricultural production has occurred on abandoned areas in Russia during 2006–2009. And even after that, the Russian government adopted policies to support the recultivation of abandoned lands (e.g., by banning agricultural imports from the EU in 2014)<sup>46</sup>.

The current war between Russia and Ukraine, however, could lead to a new wave of cropland abandonment, reduce the rate of recultivation and thus increase the carbon sink in areas of the

conflict region. Such effects of conflicts on agricultural land use could already be observed during the Chechen wars in Russian north Caucasus<sup>47</sup>. In contrast, the current rise in food prices and sanctions being placed on trade<sup>48</sup> could press the Russian government to increase domestic agricultural production and, thus, lead to massive recultivation of abandoned areas in Russia. This scenario would have a significant impact on the Eastern European carbon budget and would lead to an amplification of the declining trend of the land carbon sink in the near future.

The trend in the net carbon flux from land use change went from a recognizable sink of  $0.04 \text{ Gt C a}^{-1} \pm 0.01 \text{ Gt C a}^{-1}$  towards near neutral during 2010–2019 (see Supplementary Fig. 2). In BLUE, besides the declining carbon uptake from agricultural abandonment, an increase in emissions from forest harvest contributes to the overall decreasing trend. This underlines the importance of land management in addition to the often better investigated land use-induced land cover changes and stresses the need for monitoring of land management in addition to land cover changes<sup>49</sup>. Based on a random forest regression model, we find that wood harvest (the fraction of harvested forest area) is the most important anthropogenic driver of the trend in the carbon sink of European Russia during 2010–2019 (see Fig. 5b).



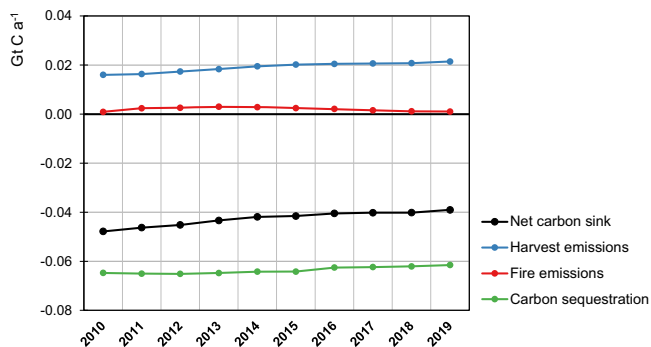


**Fig. 6 Annual carbon flux from managed forests in European Russia and its components.** Emissions from wood harvest and fire, net carbon sink (based on Russian National Inventory Reports, UNFCCC).

The growing harvest rate in European Russia and Baltic countries has also been noted by other studies<sup>27,50</sup>. Further, UNFCCC data shows that carbon losses due to clear-cutting in forests of European Russia have increased by around 34% (from 16.0 to 21.5 Mt C a<sup>-1</sup> ± 2.8 Mt C a<sup>-1</sup>, see Fig. 6).

Not only increasing carbon losses due to felling and rising logging volumes in European Russia in particular in Volga and north-western districts, have led to a decreasing carbon sink. But also, the changing age structure in the forest stands after 2008 (older stands) has decreased the carbon sink due to reduced carbon absorption<sup>45</sup>.

Our findings suggest that the rising rates of wood harvest, together with a progressive saturation of the sink from agricultural abandonment, have been the main drivers for the declining carbon sink in Eastern Europe during 2010–2019. The biomass loss due to wood harvest, however, might be partially compensated by the enhanced carbon absorption of young deciduous (or mixed-species) forest after wood harvest compared to former mature coniferous forest. If the fraction of wood harvest remains low, stand replacement after wood harvest can not only lead to an increased carbon sequestration rate (compared to old stands), it goes along with a reduction of fire risk and albedo and could have further consequences on the energy balance<sup>51</sup> and cloud cover<sup>52</sup>.

The relatively large fraction of the carbon sink explained by management (wood harvest) and land use change (agricultural abandonment) from our driver analysis (see Fig. 5) implies that anthropogenic factors likely played a dominant role in influencing AGB carbon changes in Eastern Europe. However, environmental changes, particularly soil moisture, are found to be the strongest drivers of the overall AGB carbon changes at regional level. This is consistent with other large-scale studies on attributing the carbon sink in Europe<sup>53</sup>. Environmental factors such as soil moisture and precipitation influence the carbon sink, especially in northern European Russia and along the Ural Mountains. In accordance with this, it has been shown that soil moisture variability and trends largely influences the global terrestrial carbon sink<sup>20,54</sup>. At the same time, an increase in agricultural inputs—cropland intensification in Ukraine, and southern Russia—as well as nitrogen oxides (NO<sub>x</sub>) produced during combustion have affected the land-based carbon balance in terms of an increased nitrogen deposition, which in turn stimulates vegetation productivity<sup>19</sup>. However, increased CO<sub>2</sub> concentrations have explained the rising global terrestrial carbon sink during the last three decades to a much higher extent than increased nitrogen deposition<sup>55</sup>. The effect of CO<sub>2</sub> fertilization—enhanced vegetation productivity due to increased CO<sub>2</sub> concentration—is well described as an important negative feedback on climate warming<sup>56</sup>. Recently, a global decline in the CO<sub>2</sub>

fertilization effect has been discovered, mainly affecting European forests<sup>18</sup>. The currently ongoing decrease in nitrogen deposition may still contribute to the saturation of the Eastern European forest carbon sink<sup>34</sup>.

The overall climate effect on the Eastern European carbon uptake is ambiguous. Warmer and wetter conditions in Russian boreal forests favor forest growth in the North, whereas an increasing influence of precipitation anomalies (especially drought) in southern agricultural areas, fosters a carbon source, contributes to the declining trend of the carbon sink. Future climate change projections show an ongoing decrease of precipitation in southern European Russia<sup>57</sup>.

In addition, climate change and accompanied extreme events have led to a substantial increase in forest fires and other forest disturbances. The frequency of extreme events and hydrological hazards amplified nearly three-fold in Russian forests during 2000–2018<sup>57</sup>. In this context, extensive drying out of forests as well as insect outbreaks have been registered in the northeast of European Russia and are likely to increase in the future<sup>58</sup>. Forest fires have been listed as second largest contributor of the declining carbon sink of Russian forests after wood harvest<sup>37</sup>. Findings of our random forest-based driver analysis support the strong importance of precipitation and temperature for Eastern European carbon source areas. In recent years (2018–2020), exceptionally high level of disturbances have been registered and are expected to cause a significant decrease of the Russian forest carbon sink<sup>57</sup>.

On the one hand, the analysis of indicator importance from our driver analysis (based on Shapley values) supports major hypotheses about the directed impacts of specific driver variables on the land carbon sink in Eastern Europe (see Fig. 5b and Supplementary Table 4). For instance, the lower the wood harvest rate, the higher the carbon sink. The higher the fraction of cropland abandonment, nitrogen depletion or CO<sub>2</sub> concentration, the higher the carbon sink. On the other hand, some previously unclear relationships could be illuminated in our analysis. For example, increased soil moisture shows a reinforcing influence on the carbon sink in Eastern Europe. Interestingly, the opposite appears to be true for precipitation. A strong increase in temperature has a negative effect on the Eastern European carbon sink. Fire, however, does not show a significant impact on the carbon sink or even a counterintuitive one, as higher burned area seems to enhance biomass. This may be either because forest fires and their seasonal dynamics simply cannot be adequately captured in an annually aggregated satellite product, or because fires do not (yet) play a major role in the Eastern European carbon sink.

## Conclusion

By comparing satellite-derived biomass estimates, improved carbon models and national inventory data, we estimate that Eastern Europe accounted for an above-ground biomass (AGB) carbon sink of ~0.41 Gt C a<sup>-1</sup> in 2010–2019, which is about 78% of the entire European carbon sink. Despite the important role for the European land carbon sink due to its large and dense forest areas as well as its distinct land use history induced by political upheaval, the overall Eastern European carbon sink shows a declining trend—with a ~52% decrease of net carbon uptake from the LULUCF sector in 2010–2019. Although soil moisture variability predominates as a driver of changes in AGB carbon, we find indications that land use and management changes combined with increasing natural disturbances led to the decline of the carbon sink in Eastern Europe in the past decade. Our findings suggest that a saturation effect of the regrowth in abandoned former agricultural areas, combined with an increase in wood

harvest, particularly in European Russia, as well as more frequent climate-induced forest disturbances such as droughts caused the Eastern European carbon sink to decline. Our results contribute to better understand the role of land management for climate mitigation. Since a stable and large carbon sink of Eastern European forests is essential for the European attempt to achieve net zero emissions in the future, an adapted forest management with a reliable monitoring system as well as more effective forest protection under future disturbance regimes are highly needed. This regional study shows—given the large share of Eastern Europe in the total European land-bound carbon and the overall importance of the Northern Hemisphere for the global land carbon sink—that a holistic view of the influences of climate change and the land use/management history on the carbon budget plays a central role in achieving international climate goals.

## Methods

In the following, the datasets and models used in this study are described.

### Carbon flux datasets

**CO<sub>2</sub> inversions.** We used the annual CO<sub>2</sub> flux data at a spatial resolution of 1.875° latitude × 3.75° longitude from the atmospheric inversion of the Copernicus Atmosphere Monitoring Service inversion (CAMS). We compared the CO<sub>2</sub> flux data from CAMS constrained by surface air-sample measurement (referred to as SURF) and by CO<sub>2</sub> column retrievals from two satellites (referred to as OCO2 and GOSAT).

SURF was released in 2019 and results from the assimilation of CO<sub>2</sub> surface air-sample measurements in a global atmospheric transport model over the period from 1979–2018. We used version v18r3 of SURF inversion data<sup>59</sup>.

OCO-2 is a satellite from NASA that was launched in July 2014, providing spatially dense and fine-resolution CO<sub>2</sub> column retrievals. The OCO2 data assimilates OCO-2 retrieval data into atmospheric inversion models. OCO-2 infers atmospheric CO<sub>2</sub> mixing ratios based on the absorption of CO<sub>2</sub> and O<sub>2</sub> in the atmosphere from solar radiation in the near infrared. From these measurements, the mixing ratio as a function of altitude (or pressure) is inferred using inverse methods. We used OCO2 data version FT18r1<sup>59</sup>.

GOSAT is a Japanese satellite that was launched in January 2009, and the column retrievals from GOSAT have relatively coarse-resolution data and low spatial density. The GOSAT data used in this study is a special product of the RECCAP-2 project (ESA) with LMDZ6A, the Atmospheric Component of the IPSL Climate Model.

In this study, the temporal coverage of SURF, OCO2, and GOSAT was 2010–2018, 2015–2018, and 2010–2016, respectively.

**TRENDY global models.** TRENDY is an ensemble of dynamic global vegetation models (DGVMs) in support of the Global Carbon Budget (GCB) annual assessment<sup>60,61</sup>. In this study, we used the following 15 DGVMs of the TRENDY project: CABLE-POP, CLASSIC, CLM5.0, ISAM, ISBA-CTRIP, JSBACH, JULES-ES-1p0, LPJ-GUESS, LPX-Bern, ORCHIDEE, ORCHIDEE-CNP, ORCHIDEEv3, SDGVM, VISIT, YIBs. We use the “S3 simulation” with time-varying CO<sub>2</sub>, climate, and land use forcing, as this is the simulation that captures both natural and anthropogenic dynamics.

In order to extract the AGB carbon, we obtained the gridded variable of cVeg (carbon in vegetation) from all 15 models. Additionally, the variable cRoot (carbon in roots) was used, however, it was only available for ten DGVMs. For those models without cRoot (JSBACH, JULES-ES-1p0, ORCHIDEEv3, VISIT, YIBs), we generated cRoot with the help of gridded above-/below-ground biomass ratios derived from Spawn et al.<sup>62</sup>. As a next step, we computed AGB carbon ( $C_{AGB}$ ) as

$$C_{AGB} = C_{Veg} - C_{Root}$$

with  $C_{Veg}$  as carbon in vegetation (above-ground) and  $C_{Root}$  as carbon in roots (below-ground). In this way, we calculated the change between AGB carbon of 2010 and that of 2019 for each of the 15 models (see Supplementary Fig. 5). We resampled the maps from 1° to 0.25° resolution using bilinear interpolation. In order to synthesize the information, we calculated the average across all 15 models.

**Satellite-based estimates of AGB carbon.** L-VOD: Vegetation optical depth, which represents vegetation attenuation properties, has been widely used to monitor the dynamics of vegetation above-ground carbon and water content<sup>8,63</sup>. In this study, we used the low frequency (1.4 GHz) passive microwave satellite data of L-band vegetation optical depth (L-VOD) derived from the Soil Moisture and Ocean Salinity (SMOS) with ascending (ASC) and descending (DESC) orbits, providing global measurements at a spatial resolution of 25 × 25 km with re-visiting time of 1–3 days since 2010<sup>64</sup>. The L-VOD product is available at <https://ib.remotesensing.inrae.fr/>. To avoid the effect of Radio Frequency Interference (RFI), we filtered the L-VOD data based on the root mean square of the measured and

simulated brightness temperature (RMSE-TB). After that, the filtered “best quality” data from ASC and DESC orbits were merged, and they were fitted and reconstructed using a method from Thoning et al.<sup>65</sup>. The reconstructed de-seasonalized long-term trend data were used to calculate the yearly value, which is the average of May, June, July and Aug (i.e., July 1st—centered averages). Next, the yearly values of above-ground biomass (AGB) were calculated using yearly L-VOD and the regressed relationship between AGB and L-VOD. Such regressed relationship was built using three existing reference maps, namely GlobBiomass product<sup>66</sup>, ESA CCI Biomass product<sup>67</sup> and AGB map by Avitabile et al.<sup>68</sup>. The uncertainty of the AGB changes was estimated by the standard deviation (variability across time) of the estimates using the different reference maps.

JPL: Xu et al. (2021) from the Jet Propulsion Laboratory (JPL) provided annual estimates of the live biomass of the global terrestrial ecosystems between 2000 and 2019, which are based on a bottom-up framework using machine learning techniques to synthesize ground-based forest inventories with airborne and satellite data<sup>13</sup>. We refer to the dataset here as JPL. We used the maps referred of global live woody vegetation carbon density, which are at ~10 km (0.1 degree) spatial resolution, calculated the annual changes and derived the mean annual change for the period of 2010–2019. We resampled the map of biomass carbon density change to 0.25° resolution using bilinear interpolation. Since the carbon density refers to both the above-ground and the below-ground biomass, we extracted the above-ground biomass with the help of the gridded above-/below-ground biomass ratio derived from Spawn et al.<sup>62</sup>.

WRI: The carbon flux model of Harris et al.<sup>7</sup> developed at the World Resources Institute (WRI) was modified to obtain the fluxes attributed to above-ground biomass (AGB) and carbon from 2010 to 2019. We refer to the dataset here as WRI. Net flux in this context is defined as the difference between the carbon emitted and removed by woody vegetation, set as areas with over 30% tree cover of the global forest change data by Hansen et al.<sup>69</sup>. Note that in contrast to L-VOD and JPL, which consider AGB from all vegetation, WRI refers to forests only. In particular, we modified the AGB map input, using the 2010 CCI Biomass map<sup>67</sup> adjusted for potential systematic differences when compared with plot-based reference data<sup>70</sup>. We also changed all inputs and variables originally set for 2000 into our baseline year 2010 such as the primary forest and tree cover datasets. We further modified the original model to exclude fluxes from other gases aside from CO<sub>2</sub> and remove carbon components from below-ground and soil. The resulting carbon flux was divided by a factor of 0.49 to derive the AGB.

The tool *Plot2Map* (<https://github.com/arnanaraza/PlotToMap>) which implements the AGB map assessment framework<sup>70</sup> was used to adjust for the systematic differences in the 2010 CCI Biomass map. The framework implements a model-based approach that makes use of a worldwide database of reference AGB with uncertainty estimates as basis for modeling spatial uncertainties of the AGB map at aggregated levels, i.e., 1 km.

**UNFCCC inventories.** The United Nations Framework Convention on Climate Change (UNFCCC) provides data from the national greenhouse gas (GHG) inventories submitted by countries that are Parties to the Convention. For comparing the land carbon uptake of the countries in Eastern Europe, we used GHG inventories referring to net CO<sub>2</sub> emissions/removals from land use, land use change, and forestry (LULUCF). We collected the data from the national inventories submitted to the UNFCCC. We acquired a complete time series from 1990 to 2019 (annual emissions) for Annex I countries Belarus, Bulgaria, Czech Republic, Estonia, Hungary, Latvia, Lithuania, Poland, Romania, Slovakia, and Ukraine from the UNFCCC website<sup>71</sup>. For Moldova (Annex II country), inventory data was only available up to the year 2013. In order to obtain the GHG inventory data for the region of European Russia, we acquired the national inventory reports (NIR) of Russia for all years from 2010 to 2019<sup>72</sup>, extracted and summed up the AGB carbon balance of managed forests from UNFCCC data for 54 Russian districts belonging to European Russia (Ural mountains as the eastern border).

**EFISCEN.** The European Forest Information SCENario Model (EFISCEN) is a large-scale model for estimating forest resource development in Europe. The model uses National Forest Inventory data as a main input. By using biomass expansion factors, stem wood volume is converted into biomass and subsequently to carbon stocks of trees. It includes a detailed dynamic growth module, while natural mortality and harvesting are included as regimes, depending on the region. For this study, EFISCEN data for 2010–2018 was acquired and used in the same version as from the European VERIFY project<sup>5</sup>.

**CBM.** The Carbon Budget Model developed by the Canadian Forest Service (CBM-CFS3) simulates the forest carbon dynamics under different scenarios of harvest and natural disturbances (fires, storms). The CBM has been validated by the Joint Research Centre of the European Commission (JRC) and adapted to forests in Europe. Forest stands are described by area, age and land use classes, and other parameters. Yield tables specify the merchantable volume production for each species, while allometric equations convert merchantable volume production into above-ground biomass at the stand level. The model provides annual data on net primary production (NPP), carbon stocks, and fluxes, as the annual C transfers

between pools and to the forest product sector. For this study, CBM data for 2010–2015 was acquired from and used in the same version as in the European VERIFY project<sup>5</sup>.

**Estimating the land-based carbon sink.** We estimated the average land carbon flux (in  $\text{Gt C a}^{-1}$ ) from inversions (SURF, GOSAT, OCO2), AGB sink estimates (L-VOD, JPL, WRI), forest ecosystem models and inventories (EFISCEN, CBM, UNFCCC) and land use bookkeeping model BLUE for different regions in Europe between 2010 and 2019. For this, we derived the annual land carbon flux estimates and calculated a multi-year average. The standard deviation was used as a measure of uncertainty and displayed as error bars in Fig. 2. For AGB biomass estimates available as annual maps, we first computed the annual AGB changes between two years. Then, the multi-year average AGB change was derived. Again, the standard deviation was used as an uncertainty measure. This was performed for different regions of Europe, defines as:

- EUR-North: Denmark, Finland, Iceland, Norway, Sweden
- EUR-West: Austria, Belgium, France, Germany, Ireland, Liechtenstein, Switzerland, United Kingdom of Great Britain and Northern Ireland, Luxembourg, Netherlands
- EUR-South: Croatia, Cyprus, Greece, Italy, Malta, Monaco, Portugal, Slovenia, Spain
- EUR-East: Belarus, Bulgaria, Czechia, Estonia, Hungary, Latvia, Lithuania, Moldova, Poland, Romania, Slovakia, Ukraine
- European Russia: Russia up to the Ural mountains as the eastern border

For the scope of this study, Eastern Europe consists of EUR-East and European Russia.

**Mapping AGB carbon change.** We calculated the agreement between AGB carbon changes in 2010–2019 between L-VOD, JPL, and WRI. TRENDY was excluded from the analysis due to its coarser spatial resolution, large inter-model deviations and relative distance to observational data streams (see Supplementary Fig. 4 for a comparison of TRENDY with L-VOD, JPL and WRI). The level of agreement was derived pixel-wise for either a carbon source or sink across Eastern Europe. We analyzed the statistical distribution of the AGB carbon change maps for each of the used datasets. Thresholding was applied by visual interpretation of the histograms. Accordingly, sources were defined by AGB below a negative threshold in  $\text{Mg C ha}^{-1} \text{ a}^{-1}$ , sinks by AGB above a positive threshold in  $\text{Mg C ha}^{-1} \text{ a}^{-1}$ .  $\Delta\text{AGB}$  values that are between the negative and the positive threshold were treated as no change or only minor change. The number of agreeing datasets was derived for each pixel as levels of agreement. Only including levels of agreement from 2 to 3 (at least two datasets agree on either a carbon source, sink or no/minor change), the average AGB carbon change was derived from the agreeing datasets. This leads to a harmonized map of AGB change in 2010–2019 based on L-VOD, JPL, and WRI.

We tested the usage of different AGB carbon change thresholds in  $\text{Mg C ha}^{-1} \text{ a}^{-1}$  for defining carbon sinks and sources with a sensitivity analysis. The used thresholds were: 0, 0.001, 0.005, 0.01, 0.05, 0.1, 0.5. Supplementary Fig. 6 shows both the maps with the dataset agreement and the maps with the derived harmonized AGB carbon change for each of those thresholds.

#### Datasets used as driver indicators of AGB carbon change

**Land use-based carbon fluxes (BLUE).** The Bookkeeping of Land-Use Emissions model (hereafter BLUE; see ref. 73, for documentation) is one of three bookkeeping models used in the Global Carbon Budget<sup>1</sup> for estimating the net  $\text{CO}_2$  flux from land use/cover change. In BLUE, transformations of natural vegetation to agriculture (cropland, pasture) and back, including gross transitions at the sub-grid scale, are considered as well as degradation from rangeland dynamics and wood harvesting. The temporal evolution of carbon gains or losses after transformations or harvesting events is based on response curves derived from literature. These response curves describe the decay of vegetation and soil carbon, including the transfer to product pools of different lifetimes, the carbon uptake due to regrowth of vegetation, and the subsequent refilling of soil carbon pools. Response curves in BLUE depend on literature-based carbon densities, which are implemented for 11 different plant functional types.

For this study, BLUE estimates based on the Historic Land Dynamics Assessment+ (HILDA+) have been used as described by Ganzenmüller et al.<sup>74</sup>. HILDA+ is a global dataset of annual land use/cover change between six land use categories (urban, cropland, pasture/rangeland, forest, unmanaged grass/shrubland, no/sparse vegetation). It is publicly available<sup>75</sup>, covers the period from 1960 to 2019 and has a spatial resolution of  $1 \text{ km}^2$ .

We used the net carbon sink from BLUE (BLUE net) as the total of all emissions from agricultural expansion (carbon source), wood harvest (carbon source), and agricultural land abandonment (carbon sink). Additionally, we used the gross carbon sink from BLUE (BLUE gross), which refers to the carbon uptake by agricultural land abandonment only.

**Forest harvest (JRC).** The dataset represents a forest harvest annual time-series from 2001 to 2019<sup>50</sup>. Forest harvest is expressed as the percentage of forest area affected by management practices per year in a  $0.2^\circ$  grid cell ( $\sim 20 \text{ km}$ ), excluding

forest losses due to fires, major windstorms, and areas with sparse forest cover. The dataset relies on the Global Forest Change (GFC)<sup>69</sup> product (version 1.8), a time-series analysis of the Landsat archive characterizing tree cover extent in the year 2000, and annual forest loss with a spatial resolution of about 30 m. Due to the spatial scale of the GFC dataset, small-scale silvicultural practices such as thinning or selective logging that may not be seen by the satellite could not be fully detected as forest loss.

First, a tree cover threshold of 20% was used to define a ‘forest’ from the GFC tree cover product. Then, a spatial aggregation to  $0.2^\circ$  was performed and the annual forest harvest was computed as the ratio between the area of forest loss and the area of forest cover, within each grid cell. Areas with sparse forest cover—that is, where forest cover in a grid cell of  $0.2^\circ$  is less than 10%—were excluded. Regions affected by forest fires, as detected by the ESA Fire Climate Change Initiative (Fire CCI version 5.1<sup>77</sup>) dataset collection, were masked out from the analysis. In the same way, in regions where the annual percentage of forest loss is greater than a given threshold, the forest loss was attributed to wind-throw and masked out. This was done under the assumption that major windstorms generally cause larger losses than those caused by forest management. The forest harvest dataset was generated using Google Earth Engine.

To account for and harmonize different forest definitions in datasets used in this study (e.g., 20% tree cover threshold here but 30% in WRI-based AGB), we used the land use/cover map of 2010 from the HILDA+ dataset<sup>76</sup>, which is based on the 30% tree cover definition. We set forest harvest to 0 outside the HILDA+ forest areas.

**Cropland abandonment.** The cropland abandonment dataset we used for this study is a synthesis map from three different data sources:

1. Abandoned arable land by Lesiv et al.<sup>78</sup>: The dataset covers the former Soviet Union, refers to the year  $\sim 2010$ , and has a spatial resolution of 10 arc-seconds. Abandoned arable land is defined as land that was previously cultivated (agricultural land) but has not been utilized for more than 5 years.
2. Farmland abandonment by Estel et al.<sup>28</sup>: Abandoned areas were classified based on MODIS Normalized Difference Vegetation Index (NDVI) time series in 2001–2012. The dataset has a spatial resolution of  $232 \text{ m}$  and covers Europe, including European Russia. We utilized the map of abandonment based on the following definition: At least three active cropland years during 2001–2006 were followed by five or six fallow years during 2007–2012.
3. HILDA+ cropland abandonment map: All areas where cropland has been converted into unmanaged grass/shrubland or forests during 2010–2019 have been classified as abandoned cropland based on HILDA+ annual land use/cover transitions maps<sup>76</sup>. The dataset has global coverage and a spatial resolution of  $\sim 1 \text{ km}$ .

All three maps were reclassified to binary mask format, with 1 representing abandoned cropland and 0 representing all other areas. The binary masks were resampled to  $0.25^\circ$  resolution using bilinear interpolation and converted to floating point values. The resulting maps depict the fractions of abandoned cropland, respectively. Finally, we derived the mean fraction of abandoned cropland per pixel from all available datasets (for former Soviet Union: Lesiv et al., Estel et al., HILDA+; for non-former Soviet Union: Estel et al., HILDA+). The resulting map of abandoned cropland represents the maximum fraction of a grid area affected by cropland abandonment during 2010–2019. It should not be used to measure abandonment in absolute terms.

**Fire.** FireCCI151 from the ESA CCI Fire project was used to derive the change in burned area/fire between 2010 and 2019. This is based upon data from the MODIS instrument on-board the TERRA satellite at  $250 \text{ m}$  resolution for the period 2001–2020<sup>77</sup>. Burned area represents the sum of area (in  $\text{m}^2$ ) of all pixels detected as burned within each grid cell and period. From this data, we cannot distinguish whether fires are naturally induced or anthropogenic. As next step, we derived the annual sums of the monthly gridded data and derived the mean annual change of burned area during 2010–2019. Finally, we resampled the map to  $0.25^\circ$  resolution using bilinear interpolation.

**Soil moisture.** Estimates of soil moisture from the Copernicus Climate Change Service (C3S) v20201 are based on the ESA Climate Change Initiative soil moisture version 03.3 and represents the current state-of-the-art for satellite-based soil moisture climate data record production<sup>79</sup>. We extracted the monthly maps of volumetric soil moisture in  $\text{m}^3 \text{ m}^{-3}$ , converted them to annual means, and derived the annual change between 2010 and 2019. Subsequently, we resampled the map to  $0.25^\circ$  resolution using bilinear interpolation.

**Precipitation.** We used gridded monthly precipitation from the TerraClimate data of monthly climate and climatic water balance for global terrestrial surfaces from 1958–2019 ( $\sim 4\text{-km}$  spatial resolution)<sup>80</sup>. From this, we derived the difference between the annual precipitation sums in 2010 and 2019 (in mm) and resampled the map to  $0.25^\circ$  resolution using bilinear interpolation.

**Temperature.** We acquired the Berkeley Earth gridded monthly surface air temperature at  $1^\circ$  spatial resolution<sup>81,82</sup> to account for temperature as a potential driver



of AGB carbon change. We derived the difference of the mean annual temperature from 2019 and 2010 and resampled the map to a 0.25° resolution using bilinear interpolation.

**CO<sub>2</sub> concentration.** To address the potential effect of CO<sub>2</sub> fertilization, we acquired monthly gridded data of the atmospheric CO<sub>2</sub> concentration as column-mean molar fraction from CAMS global greenhouse gas reanalysis (EGG4)<sup>83</sup>, which covers the period of 2003–2021. We first derived annual means from the monthly column-mean molar fraction of CO<sub>2</sub> (in ppm) for the period of 2010–2019. Second, we calculate the mean annual change in CO<sub>2</sub> flux for the entire period and resampled the map from a 0.75° to a 0.25° resolution using bilinear interpolation.

**Nitrogen deposition.** We acquired global estimates of inorganic nitrogen deposition for six individual years in the periods of 2004–2006 and 2014–2016 (2° × 2.5° grid resolution) simulated with GEOS-Chem<sup>84</sup>. The spatially explicit information provided in tables containing values of inorganic nitrogen deposition in kg km<sup>-2</sup> was first converted to point shape files and subsequently transformed into geotiff raster files. For each 3 year-period, the multi-year mean was derived. The difference between the nitrogen deposition maps of ~2015 and ~2005 was calculated and transformed into an annual rate of nitrogen deposition change in kg ha<sup>-2</sup> year<sup>-1</sup>. The map was resampled to a 0.25° resolution using bilinear interpolation. Note that the map of nitrogen deposition change, as used for the driver analysis, does not exactly cover the period from 2010 to 2019 and, thus, the effect of nitrogen deposition on ABG carbon change cannot be analyzed in its full details.

**Driver analysis.** In order to identify the major drivers of AGB carbon change in Eastern Europe, we carried out a driver analysis in two steps.

**Trend pattern matching.** In a first step, we used the standardized trends—the change between 2010 and 2019—of each of the potential driver indicators (carbon fluxes attributed to agriculture *BLUE-agr*, abandonment *BLUE-aban* and wood harvest *BLUE-harv*; fraction of cropland abandonment; wood harvest; fire; soil moisture; precipitation; temperature; CO<sub>2</sub> concentration; nitrogen deposition). Note that for cropland abandonment, not the change but the maximum fraction of abandoned land during ~2000–2019 (see previous section on cropland abandonment) was used to account for the effect of formerly abandoned cropland, since carbon sequestration can persist for several years after abandonment<sup>85</sup>. In order to assign a major driver indicator to each grid cell, hypotheses about the relationship between the driver indicators and AGB carbon change were used (see Supplementary Table 4).

A raster stack was built from the driver indicator layers, each for AGB carbon sink and source. The values of each driver indicator were standardized to a range between -1 and +1, with the exception of *abandonment* ranging from 0 to 1 (abandonment was not used as a change indicator). According to the hypothesized relations (see Supplementary Table 4), the values of driver indicators with a negative relationship were inverted (multiplied by -1). When the relationship was unclear, as for temperature, precipitation, and soil moisture, the absolute value from the values was taken for classification so that both negative and positive changes were considered equally. In both the AGB carbon sink and the AGB source stack, the driver indicator with the maximum value was identified for each grid cell. This driver indicator was assigned to the respective grid cell. As a consequence, for each AGB carbon sinks and sources (based on the average AGB carbon change from L-VOD, JPL, and WRI), the driver indicators that showed the strongest trend constrained by its relation could be identified and mapped across Eastern Europe.

**Random forest model.** In a second step, independently from the trend pattern matching, we applied a random forest regression model in order to derive the importance of the driver indicators in explaining the distribution of the AGB carbon change in Eastern Europe. All the eleven driver indicators in their full range were used as predictors, the average AGB carbon change from L-VOD, JPL, and WRI agreement (see previous section on Mapping AGB carbon change) was used as a target variable.

The random forest regression model was applied using *scikit-learn*, a machine learning library in Python 3.10. The random forest regression was run for three different subsets based on the target variable. Subset 1: AGB carbon source only, Subset 2: AGB carbon sink only, Subset 3: all AGB change values (including grid cells of the agreement but classified as “no change”).

For all runs, the dataset was split into test and train subset, where the test subset was set as 25% of the dataset. The values of all predictors were standardized and scaled between -1 and 1. To derive the optimal number of decision trees used by the model, we iteratively trained the model by using 10 to 200 trees in a 10-tree interval. The number of trees in the model yielding the best performance was taken and implemented in the final model run (see Supplementary Fig. 7). Performance of the model was measured with the R-Squared (R<sup>2</sup>) as the proportion of variance in the target variable that can be explained by the predictors.

We used Shapley values—a method from coalitional game theory—to rank the importance of the driver variables and to analyze their influence (including its direction; see Fig. 5b) on the AGB carbon change. For this, we used the SHAP (SHapley Additive exPlanations; <https://shap.readthedocs.io/>) library in Python

3.10. Shapley values are calculated by measuring the average mean of differences observed from all feature combinations. The computed mean absolute Shapley values describe how important the driver indicators are for the random forest model by measuring their overall influence. To achieve this, the average marginal contribution is determined. This approximates how important the driver indicators are in the data. The Shapley value shows the average contribution of a feature value to the prediction in different coalitions. With this, we could not only rank the driver indicators by their importance but also analyze the type and direction of impact (see Fig. 5b).

Since the harmonized AGB carbon change map builds on a threshold for defining agreement and disagreement of the original datasets (L-VOD, JPL, and WRI) and it was used as a target variable in the random forest-based driver analysis, we tested the effect of different thresholds on the model performance metrics and the resulting feature importance. We used the following thresholds: 0, 0.001, 0.005, 0.01, 0.05, 0.1, 0.5. Supplementary Table 5 displays the different sample sizes and model performance as R<sup>2</sup> and RMSE (root mean-square error). Supplementary Fig. 8 gives an overview of the Shapley value-based feature importance.

## Data availability

All input data used in this study are publicly available and their references are included in this article. Datasets generated during and/or analyzed during the current study (maps, codes, and tables) can be accessed through the corresponding author's GitHub repository: [https://github.com/karina-wink/Eastern\\_Europe\\_AGB-carbon](https://github.com/karina-wink/Eastern_Europe_AGB-carbon).

## Code availability

Codes used for generating the results of this study, i.e. the random forest-based driver analysis carried out in Python 3.10, can be accessed through the corresponding author's GitHub repository: [https://github.com/karina-wink/Eastern\\_Europe\\_AGB-carbon](https://github.com/karina-wink/Eastern_Europe_AGB-carbon). All maps were generated using QGIS 3.28.3.

Received: 7 September 2022; Accepted: 14 June 2023;

Published online: 03 July 2023

## References

- Friedlingstein, P. et al. Global carbon budget 2021. *Earth Syst. Sci. Data* **14**, 1917–2005 (2022).
- IPCC. Climate Change 2022: Mitigation of Climate Change. Intergovernmental Panel on Climate Change Working Group III contribution to the Sixth Assessment Report. <https://www.ipcc.ch/report/ar6/wg3/> (2022).
- Deng, Z. et al. Comparing national greenhouse gas budgets reported in UNFCCC inventories against atmospheric inversions. *Earth Syst. Sci. Data* **14**, 1639–1675 (2022).
- Griscom, B. W. et al. Natural climate solutions. *Proc. Natl. Acad. Sci.* **114**, 11645–11650 (2017).
- Petrescu, A. M. R. et al. The consolidated European synthesis of CO<sub>2</sub> emissions and removals for the European Union and United Kingdom: 1990–2018. *Earth Syst. Sci. Data* **13**, 2363–2406 (2021).
- Eggleston, H. S., Buendia, L., Miwa, K., Ngara, T. & Tanabe, K. 2006 IPCC guidelines for national greenhouse gas inventories. (2006).
- Harris, N. L. et al. Global maps of twenty-first century forest carbon fluxes. *Nat. Clim. Change* 1–7 <https://doi.org/10.1038/s41558-020-00976-6> (2021).
- Liu, Y. Y. et al. Recent reversal in loss of global terrestrial biomass. *Nat. Clim. Change* **5**, 470–474 (2015).
- Wigneron, J.-P. et al. Tropical forests did not recover from the strong 2015–2016 El Niño event. *Sci. Adv.* **6**, eaay4603 (2020).
- Bloom, A. A., Exbrayat, J.-F., Velde, I. R., van der, Feng, L. & Williams, M. The decadal state of the terrestrial carbon cycle: global retrievals of terrestrial carbon allocation, pools, and residence times. *PNAS* **113**, 1285–1290 (2016).
- Sitch, S. et al. Evaluation of ecosystem dynamics, plant geography and terrestrial carbon cycling in the LPJ dynamic global vegetation model. *Glob. Change Biol.* **9**, 161–185 (2003).
- Grassi, G. et al. Harmonising the land-use flux estimates of global models and national inventories for 2000–2020. *Earth Syst. Sci. Data* **15**, 1093–1114 (2023).
- Xu, L. et al. Changes in global terrestrial live biomass over the 21st century. *Sci. Adv.* **7**, ea9829 (2021).
- Houghton, R. A. & Nassikas, A. A. Global and regional fluxes of carbon from land use and land cover change 1850–2015. *Glob. Biogeochem. Cycles* **31**, 456–472 (2017).
- Schierhorn, F. et al. Post-Soviet cropland abandonment and carbon sequestration in European Russia, Ukraine, and Belarus. *Glob. Biogeochem. Cycles* **27**, 1175–1185 (2013).



16. Fuchs, R. et al. Assessing the influence of historic net and gross land changes on the carbon fluxes of Europe. *Global Change Biol.* **22**, 2526–2539 (2016).
17. Pilli, R., Grassi, G., Kurz, W. A., Fiorese, G. & Cescatti, A. The European forest sector: past and future carbon budget and fluxes under different management scenarios. *Biogeosciences* **14**, 2387–2405 (2017).
18. Wang, S. et al. Recent global decline of CO<sub>2</sub> fertilization effects on vegetation photosynthesis. *Science* **370**, 1295–1300 (2020).
19. Tharammal, T., Bala, G., Devaraju, N. & Nemani, R. A review of the major drivers of the terrestrial carbon uptake: model-based assessments, consensus, and uncertainties. *Environ. Res. Lett.* **14**, 093005 (2019).
20. Humphrey, V. et al. Soil moisture–atmosphere feedback dominates land carbon uptake variability. *Nature* **592**, 65–69 (2021).
21. Ciais, P. et al. Five decades of northern land carbon uptake revealed by the interhemispheric CO<sub>2</sub> gradient. *Nature* **568**, 221–225 (2019).
22. Reuter, M. et al. Satellite-inferred European carbon sink larger than expected. *Atmos. Chem. Phys.* **14**, 13739–13753 (2014).
23. Reuter, M. et al. How much CO<sub>2</sub> is taken up by the European terrestrial biosphere? *Bull. Amer. Meteor. Soc.* **98**, 665–671 (2017).
24. Monteil, G. et al. The regional European atmospheric transport inversion comparison, EUROCOM: first results on European-wide terrestrial carbon fluxes for the period 2006–2015. *Atmos. Chem. Phys.* **20**, 12063–12091 (2020).
25. Scholze, M. et al. Mean European carbon sink over 2010–2015 estimated by simultaneous assimilation of atmospheric CO<sub>2</sub>, soil moisture, and vegetation optical depth. *Geophys. Res. Lett.* **46**, 13796–13803 (2019).
26. Kuemmerle, T. et al. Forest transitions in Eastern Europe and their effects on carbon budgets. *Glob. Change Biol.* **21**, 3049–3061 (2015).
27. Potapov, P. V. et al. Eastern Europe's forest cover dynamics from 1985 to 2012 quantified from the full Landsat archive. *Remote Sens. Environ.* **159**, 28–43 (2015).
28. Estel, S. et al. Mapping farmland abandonment and recultivation across Europe using MODIS NDVI time series. *Remote Sens. Environ.* **163**, 312–325 (2015).
29. Lindroth, A. et al. Storms can cause Europe-wide reduction in forest carbon sink. *Glob. Change Biol.* **15**, 346–355 (2009).
30. Bellassen, V. & Luyssaert, S. Carbon sequestration: managing forests in uncertain times. *Nature* **506**, 153–155 (2014).
31. Schepaschenko, D. et al. Russian forest sequesters substantially more carbon than previously reported. *Sci. Rep.* **11**, 12825 (2021).
32. Fan, L. et al. Siberian carbon sink reduced by forest disturbances. *Nat. Geosci.* **16**, 56–62 (2023).
33. Pongratz, J. et al. Land use effects on climate: current state, recent progress, and emerging topics. *Curr. Clim. Change Rep.* **7**, 99–120 (2021).
34. Nabuurs, G.-J. et al. First signs of carbon sink saturation in European forest biomass. *Nat. Clim. Change* **3**, 792–796 (2013).
35. Bastos, A., Gouveia, C. M., Trigo, R. M. & Running, S. W. Analysing the spatio-temporal impacts of the 2003 and 2010 extreme heatwaves on plant productivity in Europe. *Biogeosciences* **11**, 3421–3435 (2014).
36. Schaphoff, S., Reyer, C. P. O., Schepaschenko, D., Gerten, D. & Shvidenko, A. Tamm Review: Observed and projected climate change impacts on Russia's forests and its carbon balance. *Forest Ecol. Manag.* **361**, 432–444 (2016).
37. Zamolodchikov, D. G., Grabovskii, V. I., Shulyak, P. P. & Chestnykh, O. V. Recent decrease in carbon sink to Russian forests. *Dokl Biol. Sci.* **476**, 200–202 (2017).
38. INRAE BORDAUX. INRAE BORDEAUX Soil Moisture and Vegetation products. <https://ib.remote-sensing.inrae.fr/>.
39. Jiang, F. et al. The status of carbon neutrality of the world's top 5 CO<sub>2</sub> emitters as seen by carbon satellites. *Fundam. Res.* **2**, 357–366 (2022).
40. Watts, J. D. et al. Carbon uptake in Eurasian boreal forests dominates the high-latitude net ecosystem carbon budget. *Glob. Change Biol.* **29**, 1870–1889 (2023).
41. Vuichard, N., Ciais, P., Beileli, L., Smith, P. & Valentini, R. Carbon sequestration due to the abandonment of agriculture in the former USSR since 1990. *Glob. Biogeochem. Cycles* **22**, GB4018 (2008).
42. Dolman, A. J. et al. An estimate of the terrestrial carbon budget of Russia using inventory-based, eddy covariance and inversion methods. *Biogeosciences* **9**, 5323–5340 (2012).
43. Kurganova, I., Lopes de Gerenyu, V. & Kuzyakov, Y. Large-scale carbon sequestration in post-agricultural ecosystems in Russia and Kazakhstan. *CATENA* **133**, 461–466 (2015).
44. Wertebach, T.-M. et al. Soil carbon sequestration due to post-Soviet cropland abandonment: estimates from a large-scale soil organic carbon field inventory. *Glob. Change Biol.* **23**, 3729–3741 (2017).
45. Zamolodchikov, D. G., Grabovskiy, V. I. & Chestnykh, O. V. Dynamic pattern of carbon balance in the forests of federal districts of the Russian Federation. *Вопросы лесной науки* **2**, 10–10 (2019).
46. Meyfroidt, P., Schierhorn, F., Prishchepov, A. V., Müller, D. & Kuemmerle, T. Drivers, constraints and trade-offs associated with recultivating abandoned cropland in Russia, Ukraine and Kazakhstan. *Glob. Environ. Change* **37**, 1–15 (2016).
47. Yin, H. et al. Agricultural abandonment and re-cultivation during and after the Chechen Wars in the northern Caucasus. *Glob. Environ. Change* **55**, 149–159 (2019).
48. Wegren, S. K. Sanctions likely to derail the trajectory of Russia's agricultural sector. *Political Regime Stability/Universities/Agriculture* **29**, 22 (2022).
49. Pongratz, J. et al. Models meet data: challenges and opportunities in implementing land management in Earth system models. *Glob. Change Biol.* **24**, 1470–1487 (2017).
50. Ceccherini, G. et al. Abrupt increase in harvested forest area over Europe after 2015. *Nature* **583**, 72–77 (2020).
51. Duveiller, G., Hooker, J. & Cescatti, A. The mark of vegetation change on Earth's surface energy balance. *Nat. Commun.* **9**, 679 (2018).
52. Duveiller, G. et al. Revealing the widespread potential of forests to increase low level cloud cover. *Nat. Commun.* **12**, 4337 (2021).
53. Bellassen, V. et al. Reconstruction and attribution of the carbon sink of European forests between 1950 and 2000. *Glob. Change Biol.* **17**, 3274–3292 (2011).
54. Green, J. K. et al. Large influence of soil moisture on long-term terrestrial carbon uptake. *Nature* **565**, 476–479 (2019).
55. Tagesson, T. et al. Recent divergence in the contributions of tropical and boreal forests to the terrestrial carbon sink. *Nat. Ecol. Evol.* **4**, 202–209 (2020).
56. Schimel, D., Stephens, B. B. & Fisher, J. B. Effect of increasing CO<sub>2</sub> on the terrestrial carbon cycle. *Proc. Natl. Acad. Sci.* **112**, 436–441 (2015).
57. European Forest Institute. *Russian forests and climate change*. 11 (European Forest Institute, 2020).
58. Shvidenko, A. Z. & Schepaschenko, D. G. Climate change and wildfires in Russia. *Contemp. Probl. Ecol.* **6**, 683–692 (2013).
59. CAMS. CAMS global inversion-optimised greenhouse gas fluxes and concentrations. <https://ads.atmosphere.copernicus.eu/cdsapp#!/dataset/cams-global-greenhouse-gas-inversion?tab=overview>.
60. Sitoh, S. TRENDY: Trends in the land carbon cycle | Information and data on the TRENDY project. <https://blogs.exeter.ac.uk/trendy/> (2022).
61. Sitoh, S. et al. Recent trends and drivers of regional sources and sinks of carbon dioxide. *Biogeosciences* **12**, 653–679 (2015).
62. Spawn, S. A., Sullivan, C. C., Lark, T. J. & Gibbs, H. K. Harmonized global maps of above and belowground biomass carbon density in the year 2010. *Sci. Data* **7**, 112 (2020).
63. Moesinger, L. et al. The global long-term microwave Vegetation Optical Depth Climate Archive (VODCA). *Earth Syst. Sci. Data* **12**, 177–196 (2020).
64. Wigneron, J.-P. et al. SMOS-IC data record of soil moisture and L-VOD: Historical development, applications and perspectives. *Remote Sens. Environ.* **254**, 112238 (2021).
65. Thoning, K. W., Tans, P. P. & Komhyr, W. D. Atmospheric carbon dioxide at Mauna Loa Observatory: 2. Analysis of the NOAA GMCC data, 1974–1985. *J. Geophys. Res. Atmos.* **94**, 8549–8565 (1989).
66. Santoro, M. et al. The global forest above-ground biomass pool for 2010 estimated from high-resolution satellite observations. *Earth Syst. Sci. Data* **13**, 3927–3950 (2021).
67. Santoro, M. & Cartus, O. ESA biomass climate change initiative (Biomass\_cci): global datasets of forest above-ground biomass for the years 2010, 2017 and 2018, v2. Centre for Environmental Data Analysis, 17 March 2021. <https://doi.org/10.5285/84403d09cef3485883158f4df2989b0c> (2021).
68. Avitabile, V. et al. An integrated pan-tropical biomass map using multiple reference datasets. *Glob. Change Biol.* **22**, 1406–1420 (2016).
69. Hansen, M. C. et al. High-resolution global maps of 21st-century forest cover change. *Science* **342**, 850–853 (2013).
70. Araza, A. et al. A comprehensive framework for assessing the accuracy and uncertainty of global above-ground biomass maps. *Remote Sens. Environ.* **272**, 112917 (2022).
71. UNFCCC. Greenhouse Gas Inventory Data—Time Series—Annex I. [https://di.unfccc.int/time\\_series](https://di.unfccc.int/time_series).
72. UNFCCC. National Inventory Submissions 2022 | UNFCCC. <https://unfccc.int/ghg-inventories-annex-i-parties/2022>.
73. Hansis, E., Davis, S. J. & Pongratz, J. Relevance of methodological choices for accounting of land use change carbon fluxes. *Glob. Biogeochem. Cycles* **29**, 1230–1246 (2015).
74. Ganzenmüller, R. et al. Land-use change emissions based on high-resolution activity data substantially lower than previously estimated. *Environ. Res. Lett.* **17**, 064050 (2022).
75. Winkler, K., Fuchs, R., Rounsevell, M. & Herold, M. HILDA+ (Historic Land Dynamics Assessment+) global land use change between 1960 and 2015. PANGAEA, <https://doi.org/10.1594/PANGAEA.921846>. (2020).
76. Winkler, K., Fuchs, R., Rounsevell, M. & Herold, M. Global land use changes are four times greater than previously estimated. *Nat. Commun.* **12**, 2501 (2021).

77. Chuvieco, E., Pettinari, M. L., Lizundia-Loiola, J., Storm, T. & Padilla Parellada, M. ESA Fire Climate Change Initiative (Fire\_cci): MODIS Fire\_cci Burned Area Pixel product, version 5.1. <https://doi.org/10.5285/58F00D8814064B79A0C49662AD3AF537> (2018).
78. Lesiv, M. et al. Spatial distribution of arable and abandoned land across former Soviet Union countries. *Sci. Data* **5**, 1–12 (2018).
79. Copernicus Climate Change Service. Soil moisture gridded data from 1978 to present, Land Service: Soil Moisture ECV. <https://cds.climate.copernicus.eu/cdsapp#!/dataset/eu.copernicus.climate.satellite-soil-moisture?tab=overview> (2021).
80. Abatzoglou, J. T., Dobrowski, S. Z., Parks, S. A. & Hegewisch, K. C. TerraClimate, a high-resolution global dataset of monthly climate and climatic water balance from 1958–2015. *Sci. Data* **5**, 170191 (2018).
81. Berkeley Earth. Monthly Land Average Temperature (TAVG; 1753–Recent) [Dataset] <http://berkeleyearth.org/data/>. *Berkeley Earth* (2020).
82. Rohde, R. A. & Hausfather, Z. The Berkeley earth land/ocean temperature record. *Earth Syst. Sci. Data* **12**, 3469–3479 (2020).
83. CAMS. CAMS global greenhouse gas reanalysis (EGG4) monthly averaged fields. <https://ads.atmosphere.copernicus.eu/cdsapp#!/dataset/cams-global-ghg-reanalysis-egg4-monthly?tab=overview> (2021).
84. Ackerman, D., Millet, D. B. & Chen, X. Global estimates of inorganic nitrogen deposition across four decades. *Glob. Biogeochem. Cycles* **33**, 100–107 (2019).
85. Foote, R. L. & Grogan, P. Soil carbon accumulation during temperate forest succession on abandoned low productivity agricultural lands. *Ecosystems* **13**, 795–812 (2010).
86. EFI. EFISCEN | European Forest Institute. <https://efi.int/knowledge/models/efiscen> (2023).
87. Verkerk, P. J. et al. Manual for the European Forest Information Scenario model (EFISCEN 4.1). (2016).
88. Kurz, W. A. et al. CBM-CFS3: a model of carbon-dynamics in forestry and land-use change implementing IPCC standards. *Ecol. Model.* **220**, 480–504 (2009).
89. Pilli, R., Grassi, G., Kurz, W. A., Moris, J. V. & Viñas, R. A. Modelling forest carbon stock changes as affected by harvest and natural disturbances. II. EU-level analysis. *Carbon Balance Manag.* **11**, 20 (2016).

## Acknowledgements

This research has been supported by the European Commission, Horizon 2020 Framework Programme (VERIFY, grant no. 776810). We further acknowledge Dmitry Schepaschenko for sharing valuable information on carbon storage in relation to forest management and land use change in Eastern Europe. In addition, we would like to thank Tobias Kümmerle and Christian Levers for providing underlying data on farmland abandonment across Europe by Estel et al.<sup>28</sup>.

## Author contributions

Karina Winkler prepared the manuscript, and created all figures and maps. Karina Winkler processed the HILDA+ data and adapted HILDA+ to the needs of the BLUE model. Hui Yang processed and provided the L-VOD data and carried out a preliminary comparison of carbon flux estimates. Raphael Ganzenmüller carried out the pre- and

post-processing for the BLUE model and the model runs, with support from Julia Pongratz. Ana Bastos processed and provided datasets and information on fire/burned area. Richard Fuchs co-supervised and guided the progress of the study. Guido Ceccherini, Grégory Duveiller, and Giacomo Grassi processed and provided the wood harvest data. Grégory Duveiller supported the methods of the study. Giacomo Grassi prepared and provided UNFCCC data. Arnan Araza processed and provided the bias-corrected version of the WRI biomass data, with the support of Martin Herold who supervised the study. Anatoly Shvidenko provided information on land use and forest management in European Russia. Jean-Pierre Wigneron supported the L-VOD data processing. Philippe Ciais initiated, provided a concept, and guided the progress of the study. All authors interpreted and discussed the results. All authors were involved in critical revision of the manuscript, and commented on the paper.

## Funding

Open Access funding enabled and organized by Projekt DEAL.

## Competing interests

The authors declare no competing interests.

## Additional information

**Supplementary information** The online version contains supplementary material available at <https://doi.org/10.1038/s43247-023-00893-4>.

**Correspondence** and requests for materials should be addressed to Karina Winkler.

**Peer review information** *Communications Earth & Environment* thanks Yichun Xie, Jonathan Wang, and the other, anonymous, reviewer(s) for their contribution to the peer review of this work. Primary Handling Editor: Aliénor Lavergne. A peer review file is available.

**Reprints and permission information** is available at <http://www.nature.com/reprints>

**Publisher's note** Springer Nature remains neutral with regard to jurisdictional claims in published maps and institutional affiliations.



**Open Access** This article is licensed under a Creative Commons Attribution 4.0 International License, which permits use, sharing, adaptation, distribution and reproduction in any medium or format, as long as you give appropriate credit to the original author(s) and the source, provide a link to the Creative Commons licence, and indicate if changes were made. The images or other third party material in this article are included in the article's Creative Commons licence, unless indicated otherwise in a credit line to the material. If material is not included in the article's Creative Commons licence and your intended use is not permitted by statutory regulation or exceeds the permitted use, you will need to obtain permission directly from the copyright holder. To view a copy of this licence, visit <http://creativecommons.org/licenses/by/4.0/>.

© The Author(s) 2023